

# Nonlinear interferometric vibrational imaging of molecular species

Jeremy S. Bredfeldt<sup>a</sup>, Daniel L. Marks<sup>a</sup>, Claudio Vinegoni<sup>a</sup>, Selezion Hambir<sup>b</sup>, Dana Dlott<sup>b</sup>,  
Stephen Boppart<sup>\*a,c,d,e</sup>

<sup>a</sup>Beckman Institute for Advanced Sciences, University of Illinois Urbana-Champaign, 405 N. Mathews, Urbana, IL 61801;

<sup>b</sup>School of Chemical Sciences, University of Illinois Urbana-Champaign, 600 S. Mathews, Urbana, IL 61801;

<sup>c</sup>Department of Electrical and Computer Engineering, University of Illinois Urbana-Champaign, 1406 W. Green Street, Urbana, IL 61801;

<sup>d</sup>Bioengineering Program, University of Illinois Urbana-Champaign, 1406 W. Green, Urbana, IL 61801;

<sup>e</sup>College of Medicine, University of Illinois Urbana-Champaign, 506 S. Mathews, Urbana, IL 61801

\*Electronic address: boppart@uiuc.edu

## ABSTRACT

Vibrationally sensitive spectroscopic techniques are becoming important clinical tools for real-time, *in vivo* diagnostics. The molecular information made available with these techniques can provide early diagnostic signs of disease, often before morphological changes occur. We model and experimentally demonstrate a new technique for measuring optical spectroscopy signals using interferometric ranging. This new technique, nonlinear interferometric vibrational imaging (NIVI), uses principles from coherent anti-Stokes Raman scattering (CARS) spectroscopy and optical coherence tomography (OCT) to achieve cross sectional imaging of the distribution of specific molecular species within a sample. Two CARS signals are generated, one from a known reference molecular species and a second from the unknown molecules present in a sample. These coherent signals are interfered with each other using an interferometer setup. The intensity envelope of the interference signal provides a measure of the concentration of selected bonds present in the sample focal volume. The interference fringes themselves can provide phase information that will allow for the exact reconstruction of the vibrational characteristics of the molecules in the sample focal volume. Theoretical background to CARS interferometry is presented, the experimental laser systems used are shown and a depth resolved scan line of a benzene filled cuvette is demonstrated. The experimental results show close resemblance to the theoretical models. The advantages of NIVI over existing vibrational imaging systems and its clinical implications are discussed.

Keywords: Coherent anti-Stokes Raman scattering, optical coherence tomography, nonlinear, interferometer, spectroscopy

## 1. INTRODUCTION

Histopathology, although a standard medical diagnostic procedure, cannot be performed *in vivo*, is highly subjective, and requires a blind biopsy. To address these limitations, optical spectroscopy is emerging as an alternative to microscopic tissue diagnosis. In particular, spontaneous Raman scattering spectroscopy is a technique that can acquire rapid, molecular specific information about a sample based on endogenous vibrational properties. Differences in the Raman scattering spectra between normal and diseased tissue have been established for a wide variety of diseases including, but not limited to, atherosclerotic cardiovascular disease<sup>1-3</sup>, and cancers of the skin<sup>4,5</sup>, cervix<sup>6</sup>, breast<sup>7</sup>, and brain<sup>8</sup>. With the use of fiber optic based probes<sup>9</sup>, Raman spectroscopy has the potential to help direct real-time therapeutic intervention such as interoperative tumor boarder demarcation or the monitoring of the effects of certain therapies. Raman spectroscopy has also been integrated with confocal microscopy to produce high resolution three dimensional images to study the microscopic Raman properties of biological tissues<sup>10</sup>. Unfortunately, under safe illumination levels, spontaneous Raman scattering signals are extremely weak and often suffer from the presence of a strong fluorescence background. In addition, *in vivo* Raman spectroscopy probes generally cannot determine the precise spatial distribution of Raman scatterers in a sample.

Coherent anti-Stokes Raman scattering (CARS) spectroscopy, the most well known nonlinear Raman technique, has the potential to overcome many of the difficulties associated with spontaneous Raman spectroscopy<sup>11</sup>. CARS has been implemented for the analysis of a wide variety of chemical and biological systems from shocked crystalline solids<sup>12</sup> to lipid droplets in living biological cells<sup>13</sup>. Recently, significant effort has been devoted to the integration of CARS with confocal scanning microscopy to achieve high resolution, vibrational contrast images<sup>14-17</sup>. These CARS microscopy methods generally rely on confocal gating provided by high numerical aperture (NA) objective lenses and the inherent confocal nature of the nonlinear CARS process. In this paper, we simulate and experimentally demonstrate the principle of a new method called nonlinear interferometric vibrational imaging (NIVI) that alternatively uses temporal gating to achieve spectroscopic optical ranging in tissue in a manner analogous to optical coherence tomography (OCT)<sup>18-21</sup>. This development could potentially relax the need for high NA lenses, lower the high sensitivity to stray light encountered with the use of photon counting, and therefore help to promote the clinical use of this valuable spectroscopic imaging technique. Furthermore, interferometric measurement allows for the full reconstruction of the amplitude and phase of the anti-Stokes light. With properly designed illuminating radiation<sup>21-23</sup>, a large region of the amplitude and phase of the Raman spectrum can be sampled in a single brief pulse.

CARS is a non-linear, four-wave mixing process, whose energy-level diagram is shown in Fig. 1. In traditional CARS spectroscopy, a sample is illuminated with a pump laser pulse of frequency  $\omega_p$ , and a Stokes laser pulse of frequency  $\omega_s$ , which are separated by the vibrational frequency of interest  $\omega_v = \omega_p - \omega_s$ . If the sample contains a molecule with a Raman active vibrational mode at the frequency  $\omega_v$ , an anti-Stokes pulse at frequency  $\omega_{AS} = 2\omega_p - \omega_s$  is produced. The anti-Stokes field intensity is therefore linearly dependent on the Stokes field intensity and quadratically dependent on the pump field intensity.

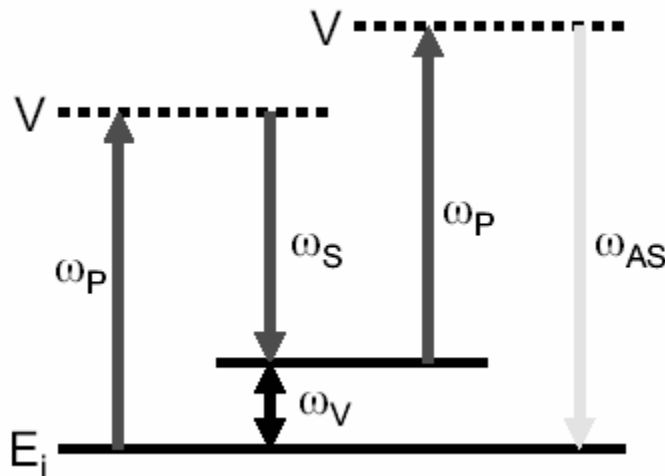


Fig. 1. Energy diagram describing the CARS process.

Since CARS is a coherent process, constructive interference of the anti-Stokes field causes the CARS signal to be significantly larger than the spontaneous Raman signal, given the same average excitation power. This allows CARS to probe the density of molecules with a particular Raman resonance frequency while exposing the specimen to relatively low levels of illumination. However, non-resonant, four-wave-mixing background signals from the Raman scatterers or the solvent often over power the resonant CARS signal when femtosecond pulses are used. The suppression of this background signal is an extremely important matter when attempting to measure resonant CARS signals. Pico second pulses have been effectively used to reduce this background signal. However, since the spatial resolution of a temporally gated interferometric technique requires the use of the shortest possible pulse, this method will not work in a high resolution optical ranging system. Fortunately, pulse shaping<sup>23</sup> has been shown to accomplish background signal suppression with the use of broad-band femtosecond pulses.

CARS is used to generate vibrational contrast in microscopy by scanning a tightly focused pump and Stokes beam through the sample while counting the anti-Stokes photons at each point. This photon count is proportional to the square

of the molecular bond density and the magnitude of the Raman susceptibility. Although a powerful technique, photon counting does not take advantage of the coherent nature of the CARS signal. NIVI exploits this coherence by measuring the interference between the sample CARS signal and another coherently generated signal at the same wavelength. We start by numerically modeling these experiments.

## 2. SIMULATIONS

A simulation of the experimental setup shown in Fig. 4 was performed. Liquid benzene was selected as the sample for its strong isolated Raman band at  $3063\text{ cm}^{-1}$ . This vibration was assumed to be a single vibration of Lorentzian profile with a much longer lifetime than the duration of the incident pulse. The incoming radiation was assumed to be two overlapped pulses of 30 nm bandwidth at 807 and 1072 nm, which created a beat frequency at the chosen Raman active vibrational mode of benzene. This incoming radiation is split into two arms and an anti-Stokes field is generated in each. Four photons are involved in the CARS process which is broken down into two stimulated Raman scattering (SRS) processes that begin and end with the molecule at the ground state. In the first SRS process, since broad band incident fields are used, each pair of frequencies that are separated by the resonance of the molecule at frequency  $\omega_r$ , will produce a nonlinear polarization in the molecule. The anti-Stokes radiation is then produced by the second SRS process when the nonlinear polarization is mixed with the incoming radiation field.

The nonlinear Raman polarization at each point in the sample was calculated as a function of time by driving it with the instantaneous intensity of the incident pulse. The resulting nonlinear polarization was then mixed with the incident field to create the anti-Stokes signal. The autocorrelation of the anti-Stokes field is then calculated as a function of the path length scanned by the reference arm. Figure 2 shows a snap shot of the CARS simulation 1000 femtoseconds after the pulse arrived at the sample.

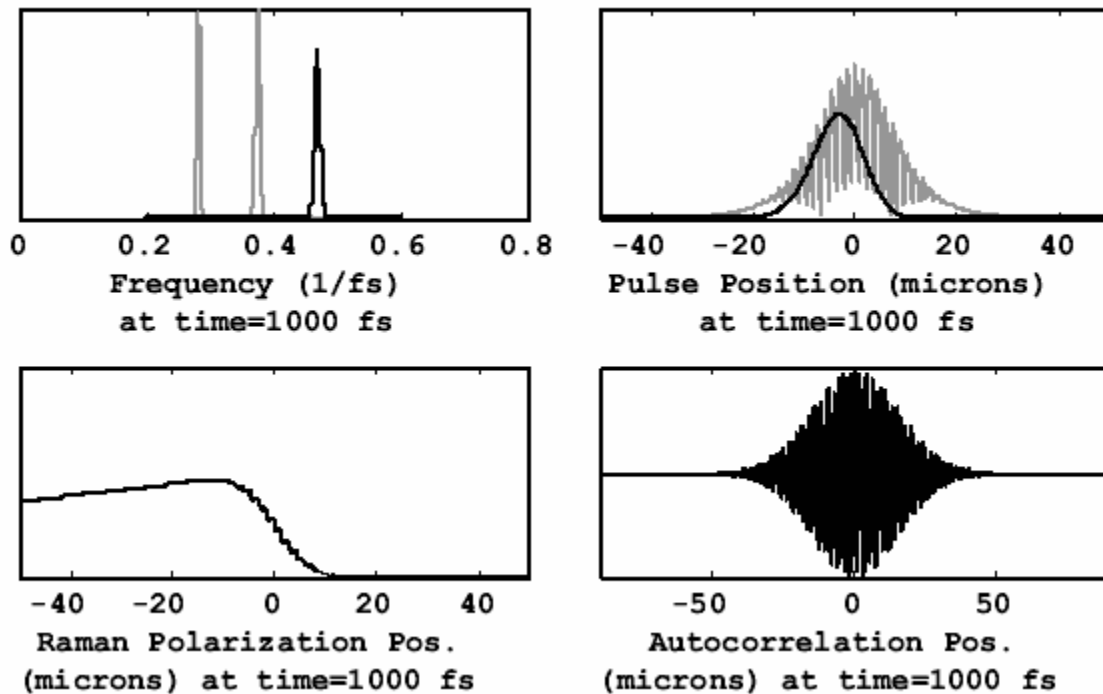


Fig. 2. Resulting CARS simulation 1000 femtoseconds after the incident pulse hits the sample.

The upper left graph of Fig. 2 shows the spectrum of the incident field in grey and the spectrum of the generated anti-Stokes field in black. The spatial profile of the incident pulse (grey) and the anti-Stokes pulse (black) is shown in the upper right graph. The lower left shows the spatial distribution of the magnitude of the Raman polarization of the benzene sample. The lower right shows the autocorrelation of the anti-Stokes pulse. Initially, when the incident pulse

first encounters the sample material, a nonlinear polarization is not excited, thus no anti-Stokes light is created. As the pulse propagates through the sample, the molecules resonate, exciting a nonlinear polarization. The incoming radiation then mixes with this polarization, creating an anti-Stokes wave at the position where the maximum Raman polarization overlaps the incident pulse. Since the anti-Stokes and incident pulses are near in frequency, and dispersion is low in the near infrared, the anti-Stokes pulse can remain in phase with the incident pulse for a long distance in the sample. Under the proposed theoretical conditions, the full width at half maximum (FWHM) of the autocorrelation is approximately 30  $\mu\text{m}$ .

### 3. EXPERIMENTAL METHODS

The laser system used to generate the excitation pulses is shown in Fig. 3. A diode pumped frequency doubled Nd:YVO<sub>4</sub> laser (Coherent, Verdi) is used to pump a mode-locked Ti:sapphire oscillator (KMLabs) operating at a center wavelength of 807 nm, with a bandwidth of 30 nm, a repetition rate of 82 MHz, and an average power of 300 mW. These low-energy oscillator pulses seed a regenerative chirped pulse amplifier (Coherent, RegA 9000) that produces approximately 70 fs, 5 uJ pulses with a repetition rate of 250 kHz and an average power of 1.25 W. Ten percent of this average power is used as the pump beam and the remaining power is directed to an optical parametric amplifier (Coherent, OPA 9400) which generates a 4 mW average power Stokes beam, tunable from 400-1200 nm.

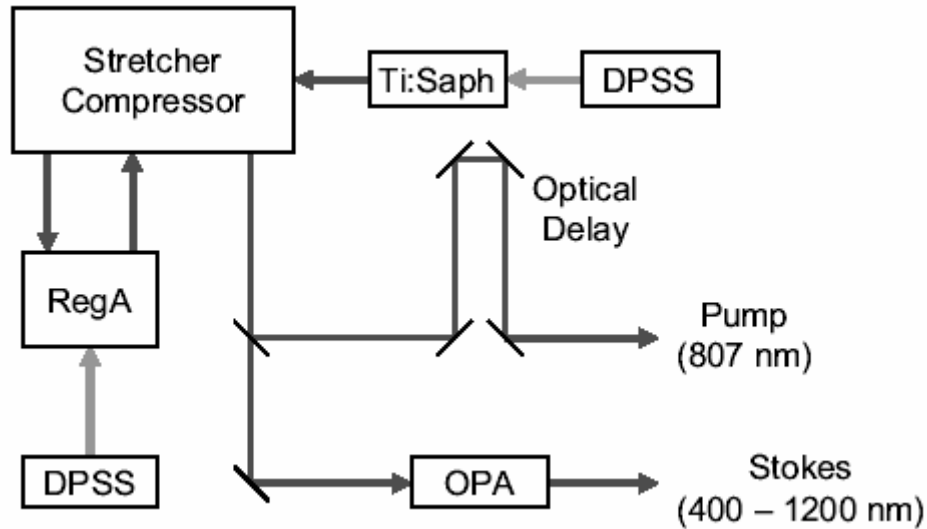


Fig. 3. Laser systems used to generate femtosecond pump and Stokes pulses. DPSS, diode-pumped solid-state; RegA, regenerative amplifier; OPA, optical parametric amplifier.

The pump and Stokes lasers, at 807 and 1072 nm respectively, are directed into the nonlinear interferometer shown in Fig. 4. These pulses are collinearly overlapped using a dichroic mirror and split with a 50:50 ultrafast beam splitter into the sample and reference arms. An anti-Stokes field is created in each arm of the interferometer. The reference arm scanning optical delay is adjusted to match the path length of the sample arm and, based on the Feynman principle, when these anti-Stokes fields are temporally and spatially overlapped, interference can be observed. The anti-Stokes field was filtered out from the excitation fields using a high-pass optical filter. As the reference arm path length is scanned, the interference signal is measured using a photomultiplier tube, electronically filtered with a low-pass anti-aliasing filter and sampled with a PC based data acquisition system.

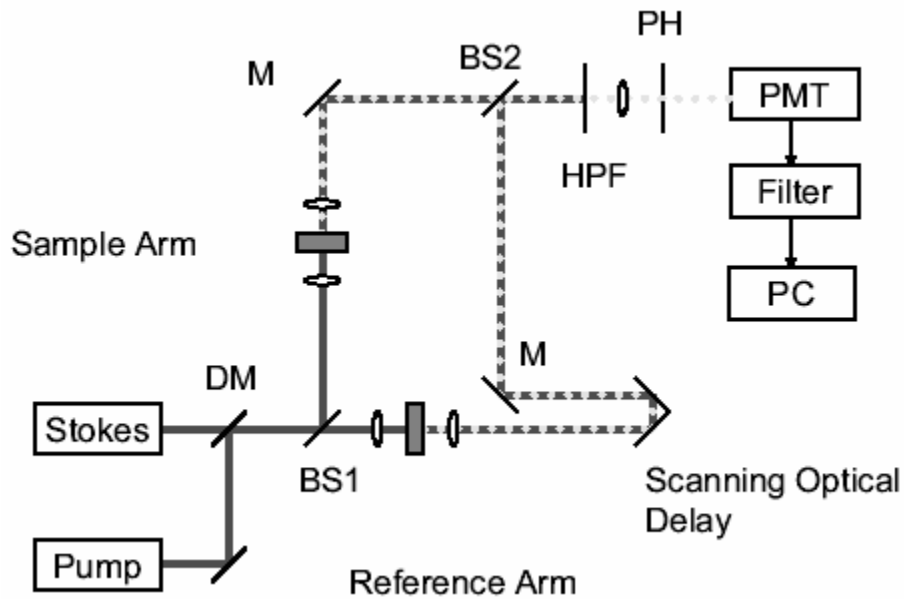


Fig. 4. Interferometric CARS measurement setup. Solid lines represent the excitation fields while the dotted line represents the CARS signal. DM, dichroic mirror; BS, beam splitter; M, mirror; HPF, high-pass-filter; PH, pin-hole; PMT, photomultiplier tube; PC, personal computer.

#### 4. EXPERIMENTAL RESULTS

To show that our signal is a result of a four wave mixing process, the relationships between the CARS and the pump intensity (Stokes intensity fixed) and the CARS and the Stokes intensity (pump intensity fixed) are observed. The resulting data are presented in Fig. 5. As indicated by the slopes of the lines fitted to the experimental data, the CARS field intensity clearly shows a quadratic relationship to the pump field intensity and a linearly relation to the Stokes field intensity.

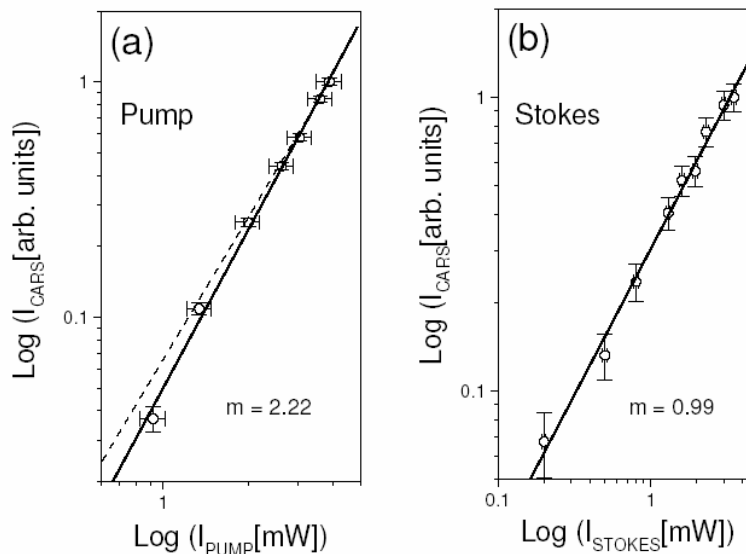


Fig. 5. Log-log plots of the intensity of the CARS signal as a function of (a) the intensity of the pump field and (b) the intensity of the Stokes field. Solid lines are the result of curve fitting. The dotted line in (a) has a slope of 2 and “m” is the angular coefficient of the solid lines.

The measured interferogram resulting from the interference between the two CARS signals produced in two benzene filled cuvettes is shown in Fig. 6. The degree of coherence function, for the case of a Gaussian spectral distribution, is used to fit the experimentally measured data. The envelope of the fringes corresponds to the modulus while the fringes themselves correspond to the real part of the degree of coherence function. Based on the full width at half maximum of the fringe envelope, the coherence length ( $L_c$ ) of the CARS pulse was measured to be 32  $\mu\text{m}$ . The inset in the lower right corner of Fig. 6 shows a zoomed version of the interference fringes, revealing the wavelength ( $\lambda_{AS}$ ) of the CARS field to be 647 nm.

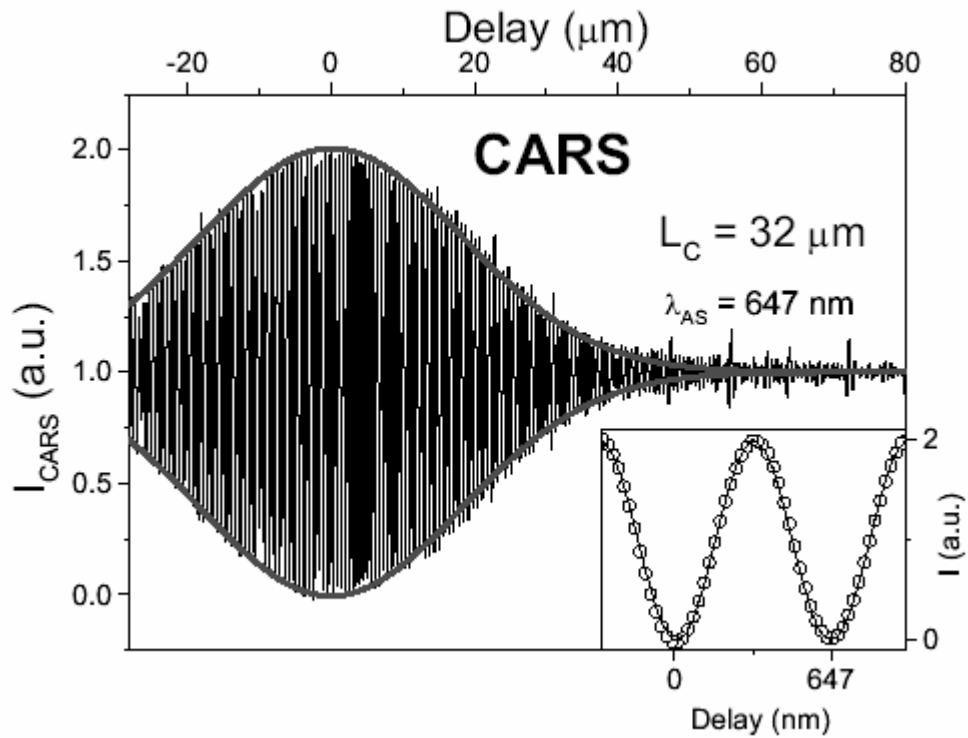


Fig. 6. CARS interferogram detected at the beam splitter BS2 of the setup shown in Fig. 2. The solid line is a fit of the envelope of the interferogram using the modulus of the degree of coherence function. A detail of the interference pattern is shown in the inset of the figure and is fit by the real part of the degree of coherence function. Open circles represent experimental data while the solid line represents the fit.  $L_c$  is the coherence length of the pulse and  $\lambda_{AS}$  is the wavelength of the CARS signal.

## 5. DISCUSSION

Excellent correspondence between the theoretical models and experimental data is observed. The linear relationship observed between the CARS and Stokes intensity and the quadratic relationship between the CARS and pump intensity matches theory exactly and clearly demonstrates that the hypothesized CARS signal is the result of a four-wave-mixing process. The presence of the CARS interferogram indicates that two CARS signals generated in separate samples of benzene can be demodulated interferometrically, where the amplitude of the fringe envelope gives information about the concentration of scatterers in the focal volume of the sample objective lens. In addition, the simulation closely predicts the experimentally observed cross-correlation between the two CARS signals. These results indicate that NIVI is a potentially useful technique for CARS measurement that can allow for the acquisition of three dimensional vibrational images in a manner similar to OCT. In addition, temporal gating relaxes the need for high NA lenses,

interferometric detection allows for heterodyne sensitivity, and with proper illumination can be used to reconstruct large portions of the Raman susceptibility in a single pulse. These advantages suggest that NIVI may be more adaptable to various scanning configurations than other vibrational spectroscopy imaging techniques and may ultimately lead to more attainable clinical applications.

## REFERENCES

1. J. J. Baraga, M. S. Feld, and R. P. Rava, "In situ chemical analysis of biological tissue: Vibrational Raman spectroscopy of human atherosclerosis," *Proc. Natl. Acad. Sci. USA* **89**, 3473-3477 (1992).
2. T. J. Romer, J. F. Brennan, M. Fitzmaurice, M. L. Feldstein, G. Deinum, J. L. Myles, J. R. Kramer, R. S. Lees, and M. S. Feld, "Histopathology of human coronary atherosclerosis by quantifying its chemical composition with Raman spectroscopy," *Circulation* **97**, 878-885 (1998).
3. S. W. van de Poll, K. Kastelijn, T. C. Bakker Schut, C. Strijder, G. Pasterkamp, G. J. Puppels, A. van der Laarse, "On-line detection of cholesterol and calcification by catheter based Raman spectroscopy in human atherosclerotic plaque ex vivo," *Heart*, **89**, 1078-1082 (2003).
4. S. Fendel, and B. Schrader, "Investigation of skin and skin lesions by NIR-FT-Raman spectroscopy," *J. Anal. Chem.* **360**, 609-613 (1998).
5. P. J. Caspers, G. W. Lucassen, G. J. Puppels, "Combined in vivo confocal Raman spectroscopy and confocal microscopy of human skin," *Biophys. J.*, **85**, 572-580 (2003).
6. A. Mahadevan-Jansen, M. F. Mitchell, N. Ramanujam, U. Utzinger, and R. Richards-Kortum, "Development of a fiber optic probe to measure NIR Raman spectra of cervical tissue in vivo," *Photochem. Photobiol.*, **68**, 427 (1998).
7. C. J. Frank, R. L. McCreery, D. C. Redd, "Raman Spectroscopy of Normal and Diseased Human Breast Tissues," *Anal. Chem.* **67**, 777-783 (1995).
8. S. Koljenovic, L. P. Choo-Smith, T. C. Bakker Schut, J. M. Kros, H. J. van den Berge, G. J. Puppels, "Discriminating vital tumor from necrotic tissue in human glioblastoma tissue samples by Raman spectroscopy," *Lab Invest.*, **82**, 1265-1277 (2002).
9. U. Utzinger, and R. R. Richards-Kortum, "Fiber optic probes for biomedical optical spectroscopy," *J. Biomed. Opt.* **8**, 121-147 (2003).
10. N. M. Sijtsema, S. D. Wouters, C. J. de Grauw, C. Otto, and J. Greve, "Confocal direct imaging Raman microscope: design and applications in biology," *Appl. Spectrosc.* **52**, 348-355 (1998).
11. R. J. H. Clark and R. E. Hester, eds., *Advances in Non-linear Spectroscopy* (Wiley, New York, 1988).
12. S. A. Hambir, J. Franken, D. E. Hare, E. L. Chronister, B. J. Baer, and D. Dlott, "Ultrahigh time resolution vibrational spectroscopy of shocked molecular solids," *J. Appl. Phys.* **81**, 2157-2166 (1997).
13. X. Nan, J.-X. Cheng, and X. S. Xie, "Vibrational imaging of lipid droplets in live fibroblast cells with coherent anti-Stokes Raman scattering microscopy," *J. Lipid. Res.* **44**, 2202-2208 (2003).
14. M. D. Duncan, J. Reintjes, and T. J. Manuccia, *Opt. Lett.* **7**, 350 (1982).
15. E. O. Potma, D. J. Jones, J.-X. Cheng, X. S. Xie, and J. Ye, *Opt. Lett.* **27**, 1168 (2002).
16. M. Muller, J. Squier, C. A. de Lange, and G. J. Brakenhoff, "CARS microscopy with folded BoxCARS phasematching," *J. Microsc.* **197**, 150-158 (2000).
17. N. Uzunbajakava, A. Lenferink, Y. Kraan, B. Willekens, G. Vrensen, J. Greve, and C. Otto, "Nonresonant Raman imaging of protein distribution in single human cells," *Biopolymers* **72**, 1-9 (2003).
18. D. Huang, E. A. Swanson, C. P. Lin, J. S. Schuman, W. G. Stinson, W. Chang, M. R. Hee, T. Flotte, K. Gregory, C. A. Puliafito, and J. G. Fujimoto, "Optical Coherence Tomography," *Science* **254**, 1178-1181 (1991).
19. S. A. Boppart, B. E. Bouma, C. Pitris, J. F. Southern, M. E. Brezinski, and J. G. Fujimoto, "In vivo cellular optical coherence tomography imaging," *Nature Medicine* **4**, 861 (1998).
20. B. E. Bouma and G. J. Tearney, eds., *Handbook of Optical Coherence Tomography* (Marcel Dekker, Inc., 2001).
21. D. L. Marks and S. A. Boppart, "Nonlinear interferometric vibrational imaging," *Phys. Rev. Lett.* submitted 2003.
22. A. M. Weiner, D. E. Leaird, G. P. Wiederrecht, K. A. Nelson, "Femtosecond pulse sequences used for optical manipulation of molecular motion," *Science* **247**, 1317-1319 (1990).
23. N. Dudovich, D. Oron, and Y. Silberberg, "Single-pulse coherent controlled nonlinear Raman spectroscopy and microscopy," *Nature* **418**, 512-514 (2002).
24. J.-X. Cheng, L. D. Book, and X. S. Xie, "Polarization coherent anti-Stokes Raman scattering microscopy," *Opt. Lett.* **26**, 1341-1343 (2001).